Published OnlineFirst October 3, 2014; DOI: 10.1158/1541-7786.MCR-14-0155

Oncogenes and Tumor Suppressors

Molecular Cancer Research

Matrix Stiffening and β_1 Integrin Drive Subtype-Specific Fibroblast Accumulation in Lung Cancer

Marta Puig[1,2], Roberto Lugo[1], Marta Gabasa[1], Alícia Giménez[1], Adriana Velásquez[1], Roland Galgoczy[1], Josep Ramírez[3], Abel Gómez-Caro[4], Óscar Busnadiego[5], Fernando Rodríguez-Pascual[5], Pere Gascón[2], Noemí Reguart[2], and Jordi Alcaraz[1,6]

Abstract

The crucial role of tumor-associated fibroblasts (TAF) in cancer progression is now clear in non–small cell lung cancer (NSCLC). However, therapies against TAFs are limited due to a lack of understanding in the subtype-specific mechanisms underlying their accumulation. Here, the mechanical (i.e., matrix rigidity) and soluble mitogenic cues that drive the accumulation of TAFs from major NSCLC subtypes: adenocarcinoma (ADC) and squamous cell carcinoma (SCC) were dissected. Fibroblasts were cultured on substrata engineered to exhibit normal- or tumor-like stiffnesses at different serum concentrations, and critical regulatory processes were elucidated. In control fibroblasts from nonmalignant tissue, matrix stiffening alone increased fibroblast accumulation, and this mechanical effect was dominant or comparable with that of soluble growth factors up to 0.5% serum. The stimulatory cues of matrix rigidity were driven by β1 integrin mechanosensing through FAK (pY397), and were associated with a post-transcriptionally driven rise in β1 integrin expression. The latter mechano-regulatory circuit was also observed in TAFs but in a subtype-specific fashion, because SCC–TAFs exhibited higher FAK (pY397), β1 expression, and ERK1/2 (pT202/Y204) than ADC–TAFs. Moreover, matrix stiffening induced a larger TAF accumulation in SCC–TAFs (>50%) compared with ADC–TAFs (10%–20%). In contrast, SCC–TAFs were largely serum desensitized, whereas ADC–TAFs responded to high serum concentration only. These findings provide the first evidence of subtype-specific regulation of NSCLC–TAF accumulation. Furthermore, these data support that therapies aiming to restore normal lung elasticity and/or β1 integrin-dependent mechano regulation may be effective against SCC–TAFs, whereas inhibiting stromal growth factor signaling may be effective against ADC–TAFs.

Implications: This study reveals distinct mechanisms underlying the abnormal accumulation of tumor-supporting fibroblasts in two major subtypes of lung cancer, which will assist the development of personalized therapies against these cells. *Mol Cancer Res; 13(1); 161–73. ©2014 AACR.*

Introduction

Non–small cell lung cancer (NSCLC) is the most frequent type of lung cancer and includes two major histologic subtypes: adenocarcinoma (ADC) and squamous cell carcinoma (SCC; ref. 1). Because these NSCLC subtypes are epithelial in origin, most previous studies have focused on neoplastic epithelial cells. However, there is growing awareness that tumor progression requires stromagenesis, that is, the formation of a supportive tumor stroma (2, 3). In NSCLC and other solid tumors, the stroma is desmoplastic, exhibiting an overabundance of tumor-associated fibroblasts (TAF), type I collagen (collagen-I) and other fibrotic extracellular matrix (ECM) components, new blood vessel formation, and immune cell infiltration (2–5). Such desmoplastic stroma supports tumor cell growth, invasion, metastasis, and even resistance to treatments (5, 6).

Developing therapies against stroma–carcinoma interactions demands identifying the key mechanisms underlying cancer stromagenesis. The current paradigm considers the latter mechanisms similar to those underlying generic wound repair, according to the striking similarities between the tissue alterations found in desmoplastic stromas and in wounds (4, 7). However, it remains ill defined whether stromagenesis is actually driven by generic repair responses or rather by cancer subtype-specific mechanisms.

Because TAFs are the most abundant stromal cell type (6), there is growing interest in unraveling the processes underlying TAF accumulation during stromagenesis. In NSCLC and other cancer types, TAFs are frequently found in an activated/myofibroblast-like phenotype that is roughly characterized by the expression of alpha-smooth muscle actin (α-SMA) and the enhanced deposition of fibrotic ECM components. In the current paradigm, TAF accumulation is assumed to be largely driven by paracrine signals secreted by cancer cells or infiltrated immune cells as in generic repair processes (3, 8–10). However, two lines of evidence suggest that mechanical cues provided by the abnormal tissue hardening

[1]Unitat de Biofísica i Bioenginyeria, Facultat de Medicina, Universitat de Barcelona, Barcelona, Spain. [2]Medical Oncology Department, Hospital Clínic de Barcelona, Institut d'Investigacions Biomèdiques August Pi i Sunyer, Barcelona, Spain. [3]Servei d'Anatomia Patològica, Hospital Clínic de Barcelona, Barcelona, Spain. [4]Servei de Cirurgia Toràcica, Hospital Clínic de Barcelona, Barcelona, Spain. [5]Centro de Biología Molecular "Severo Ochoa," CSIC, Madrid, Spain. [6]CIBER de Enfermedades Respiratorias, Bunyola, Spain.

Note: Supplementary data for this article are available at Molecular Cancer Research Online (http://mcr.aacrjournals.org/).

Corresponding Authors: Jordi Alcaraz, CIBER de Enfermedades Respiratorias, Casanova 143, Barcelona 08036, Spain. Phone: 34-93-402-4515; Fax: 34-93-403-5278; E-mail: jalcaraz@ub.edu; and Noemi Reguart, Department d'Oncologia Mèdica, Institut d'Investigacions Biomèdiques August Pi i Sunyer, Villarroel 170, Barcelona 08036, Spain, nreguart@clinic.ub.es

doi: 10.1158/1541-7786.MCR-14-0155

©2014 American Association for Cancer Research.

Downloaded from mcr.aacrjournals.org on September 15, 2015. © 2015 American Association for Cancer Research.

Published OnlineFirst October 3, 2014; DOI: 10.1158/1541-7786.MCR-14-0155

of desmoplastic tumors may also contribute to TAF accumulation. First, increasing the rigidity of culture substrata enhances the effects of exogenous growth factors on the survival and/or proliferation of fibroblasts from nonmalignant tissues (11–13). Second, a marked increase in matrix rigidity is expected in the stroma of NSCLC, because two hallmarks of desmoplastic tumors—abundant collagen-I fibers and α-SMA$^+$ fibroblasts—have been associated with dramatic tissue hardening (14–17).

We sought to determine to what extent extracellular mechanical and soluble mitogenic cues regulate the accumulation of TAFs from both major NSCLC subtypes (ADC and SCC). We found that the accumulation of ADC–TAFs in culture was mostly driven by exogenous growth factors, in agreement with a generic repair response. In contrast, the accumulation of SCC–TAFs largely required matrix stiffening, whereas it was poorly responsive to exogenous growth factors irrespective to their concentration. We also identified the critical role of β_1 integrin mechano-receptors and delineated additional key molecular aspects of the regulatory role of matrix rigidity on fibroblast density.

Materials and Methods

Tissue samples and primary human lung fibroblasts

Tissues were collected from 21 resected patients with stage I/II NSCLC at the Hospital Clinic de Barcelona (HCB; 10 ADC and 11 SCC). The study was approved by the Ethics Committees of the HCB and the Universitat de Barcelona, and all patients gave their informed consent. Selected patients were male, chemo-naïve, Caucasian, >55-years-old, and current smokers. Further clinical characteristics are given in Supplementary Table S1. Samples from tumor and paired tumor-free lung parenchyma were collected. A fraction of each sample was paraffin-embedded, and the remaining was used to isolate fibroblasts by outgrowth of tissue explants (18).

Histology

Paraffin-embedded samples were sliced in 2- to 4-μm sections, deparaffinized and rehydrated. Tissue architecture and fibrillar collagens were visualized by hematoxylin–eosin (H&E) and 0.1% picrosirius red in saturated picric acid (Direct Red 80; Sigma) stainings, respectively. Immunohistochemical analyses of β_1 integrin, α-SMA and Ki-67 were performed using the Bond automated immunohistochemistry system (Leica Microsystems). Primary antibodies included anti-β_1 integrin (M-106; Santa Cruz Biotechnology), anti–α-SMA (1A4; Dako), and anti–Ki-67 (MIB-1; Dako). H&E and immuno-stainings were imaged with a bright-field microscope (DM5000 B) coupled to a digital camera (DFC 500; Leica). Picrosirius red staining was imaged using polarized filters. All image processing henceforth was carried out with ImageJ (19). α-SMA stainings were imaged at 10 randomized locations for each patient with a ×10 objective. Each image was color deconvoluted and the α-SMA channel was binarized to calculate the α-SMA–positive (α-SMA$^+$) area fraction, which was averaged for each patient and subsequently for all patients within a subtype. To assess TAF density, a similar imaging procedure was applied to H&E stainings for each patient using a ×40 objective. Fibroblast nuclei were counted in binarized images according to preoptimized morphometric criteria, including area (16–333 μm^2), circularity (0.1–0.5), and aspect ratio (2.5–15). These criteria selected spindle-shaped nuclei, which is a common morphologic approach used to identify fibroblasts in H&E staining (20). Spindle-shaped nuclei lining blood vessels were discarded. Nuclei number per image was averaged for each patient, and subsequently averaged for all patients in each subtype. The β_1 integrin staining in fibroblasts was scored in a semiquantitative manner with methods similar to those previously reported (21). Images of the stroma of β_1 integrin stainings were acquired at 10 locations in each sample. Fibroblasts were identified using the above-mentioned morphometric criteria. β_1 integrin staining in fibroblasts was scored blind by two independent observers according to three categories (negative, weak, and strong). In average, 350 fibroblasts were counted per sample. The percentage of fibroblasts per sample in terms of β_1 integrin staining was assessed for each category and observer (coefficient of correlation $r^2 = 0.8$), and averaged to render the final category percentage per histologic subtype.

Polyacrylamide gels

Collagen-I–coated polyacrylamide (PAA) gels were obtained as reported elsewhere (11, 22). In brief, gels were prepared by mixing variable ratios of acrylamide (AA)/bis-acrylamide (BIS; Bio-Rad) to exhibit normal- (3% AA:0.22% BIS) or tumor-like (12% AA:0.45% BIS) Young's modulus. After polymerization, the gel surface was derivatized with Sulfo-SANPAH (Thermo Scientific) and coated with 0.1 mg/mL collagen-I (Millipore). Matrix rigidity was assessed by atomic force microscopy (22, 23) as 0.6 ± 0.1 and 28 ± 4 kPa for normal- and tumor-like gels, respectively (mean ± SD).

Cell culture

The human fibroblast cell line CCD-19Lu (ATCC) and primary fibroblasts were maintained in culture medium described elsewhere (18) supplemented with 1X insulin–transferrin–selenium (ITS; Gibco). Fibroblasts were used up to passage 10 (CCD-19Lu) or 6 (primary). Mouse embryonic fibroblasts (MEF) from wild-type (FAK$^{+/+}$) or FAK-deficient (FAK$^{-/-}$) mice were isolated and cultured as previously reported (24). FAK$^{+/+}$ MEFs were transduced by adenoviral infection with either wild-type FAK (Adv-FAK) or an empty vector (Adv-empty; used as control) as described elsewhere (24). Cells were cultured for 5 days unless otherwise indicated. For PAA gel experiments, lung fibroblasts were seeded at 8×10^3 cells/cm^2 in serum-free culture medium (SFM) supplemented with 0.25 μmol/L ascorbic acid (Sigma) at different FBS concentrations. MEFs were cultured in the same conditions by plating either 1.45×10^4 cells/cm^2 (FAK$^{+/+}$) or 2.8×10^4 cells/cm^2 (FAK$^{-/-}$). In 2D experiments, cells were seeded in collagen-I–coated tissue culture plastic substrata. In some experiments, fibroblasts were plated in the presence of the monoclonal β_1 integrin activity inhibitory antibody AIIB2 (kindly provided by Dr. Weaver at UCSF, San Francisco, CA), the monoclonal β_1 integrin–activating antibody TS2/16 or the control IgG1 antibody (BD Biosciences).

Cell density and spreading

The nuclei of living fibroblasts were fluorescently labeled with Hoechst 33342 (Molecular Probes). Fluorescence images were acquired with an Eclipse TE2000 microscope (Nikon) at nine randomized locations with an EM-CCD C9100a camera (Hamamatsu) using Metamorph software (Molecular Devices) and a ×10 objective. For each experiment, cell density was determined as the average nuclear density/image and normalized to that value obtained at 0% FBS in 1 kPa gels. To assess cell spreading, phase-

Downloaded from mcr.aacrjournals.org on September 15, 2015. © 2015 American Association for Cancer Research.

Published OnlineFirst October 3, 2014; DOI: 10.1158/1541-7786.MCR-14-0155

contrast images were acquired with a similar protocol and used to manually outline the contour of individual cells.

Proliferation and apoptosis

Proliferative activity was assessed by identifying replicating cells with the Click-iT EdUrd Cell Proliferation Assay (Invitrogen) following the manufacturer's instructions. Samples were incubated with 50 μmol/L EdUrd solution for 24 hours. Nuclei were counterstained with Hoechst 33342 to assess total cell number in each image. Fluorescence images were acquired at nine randomized locations with a ×20 objective. For each culture condition, EdUrd-positive cells per image were counted, normalized to the total cell number, and averaged to obtain the final percentage. To assess apoptosis, cells were fixed and permeabilized in the same conditions, blocked with 0.2% Triton X-100, 1% BSA (Sigma), and 6% FBS for 1 hour, incubated overnight with a primary antibody against cleaved caspase-3 (Cell Signaling Technology) at 4ºC, and incubated with an anti-rabbit Cy-3 (The Jackson Laboratory) secondary antibody for 2 hours. Fluorescence images were obtained with the same protocol, background corrected, and their total intensity (I) and cell number (N) were recorded. For each culture condition, I versus N data were least-squares fitted to a linear function with MATLAB (Mathworks) to assess the cleaved caspase-3 intensity per cell as the fitted slope.

Western blotting

Fibroblasts were lysed in extraction buffer (62.5 mmol/L Tris-HCl (pH 6.6), 2% SDS, 10% glycerol, and 50 mmol/L DTT) supplemented with phosphatase (Roche) and protease inhibitors (Cocktail Set I; Merck; Pefabloc, Roche). Equal protein amounts were separated on a 10% Mini-PROTEAN TGX precast gels (Bio-Rad), transferred to a polyvinylidene difluoride membrane (GE Healthcare), blocked, and incubated overnight with suitable primary antibodies, including anti-Akt and anti-Akt^{pS473} (9272 and 4060; Cell Signaling Technology), anti-FAK (610087; BD Transduction Laboratories), anti-FAK^{pY397} (700255; Invitrogen), anti-β1 integrin (610467; BD Biosciences), anti-Erk1/2, and anti-Erk1/2$^{pThr202/Tyr204}$ (9102 and 9101; Cell Signaling Technology), anti-GAPDH, and anti–α-tubulin (5174 and 2144; Cell Signaling Technology). The latter two were used as loading controls. Protein bands were labeled with peroxidase-conjugated stabilized goat anti-rabbit or anti-mouse IgG (H+L; Pierce), and visualized by chemiluminescence (SuperSignal West Pico Chemiluminescence Substrate; Pierce) in a digital imaging system (ImageQuant LAS 4000; GE Healthcare). Protein band intensities were quantified with Fujifilm Image Gauge 4.0 software and normalized to the corresponding loading control.

qRT-PCR

β_1 integrin transcription was assessed as described elsewhere (23) using TaqMan gene-specific primer pairs and probe (Applied Biosystems) for genes encoding ITGB1 (Hs00559595_m1) and POLR2A (used as a reference gene, Hs00172187_m1).

Flow cytometry

Fibroblasts were cultured in 2D in SFM for 24 hours and stimulated without or with 10% FBS for 5 days. Cells were trypsinized, fixed with ice-cold 70% ethanol (Sigma), and spin-dry at 2000 rpm for 10 minutes. Cell pellets were stained with PBS solution containing 0.5 mg/mL propidium iodide and 0.4 mg/mL ribonuclease A (RNase; Sigma). Cell-cycle analysis was performed from DNA histograms of single cells obtained by flow cytometry (LSRFortessa; BD Biosciences) as reported elsewhere (25). The percentages of cells in G_0–G_1, S, and G_2–M were assessed with FACSDiva Software v6.1.3 (BD Biosciences).

Statistical analysis

Two-group comparisons were performed with the Student t test (SigmaPlot) unless otherwise indicated. Statistical significance was assumed at $P < 0.05$.

Results

Desmoplastic tumor stroma accounts for 25% of the total tumor and exhibits markers of tissue hardening in both ADC and SCC

In normal lung parenchyma, fibroblasts were sparsely located, and α-SMA$^+$ cells corresponding to smooth muscle cells were largely restricted to the perivasculature (see black arrows). In contrast, both ADC and SCC samples exhibited a stroma rich in peritumoral α-SMA$^+$ TAFs (Fig. 1A and Supplementary Fig. S1). These features were used to assess the relative amount of tumor stroma as the percentage of α-SMA$^+$ area, which elicited approximately 25% in both ADC and SCC (Fig. 1B and Supplementary Fig. S2). Conversely, morphometric analysis revealed that TAF density was approximately 1.5-fold higher in ADC than in SCC (Fig. 1C and Supplementary Fig. S3). Ki-67 staining could not unambiguously unravel whether the latter difference was due to differential proliferation of resident fibroblasts or to other processes (Supplementary Fig. S4; ref. 26). Nonetheless, these results suggest that TAF accumulation may be driven—at least in part—by subtype-specific mechanisms. We further analyzed the stroma by examining the content of fibrillar collagens (Fig. 1A). Normal lung parenchyma exhibited weak collagen staining and short collagen fibers, whereas tumor samples from both ADC and SCC exhibited abundant collagen staining that was frequently organized into long and straight fibril bundles indicative of mechanical tension. Likewise, fibril bundles were often organized in a parallel fashion (see dashed squares), which has been previously shown to render stiffer tissues (16).

Matrix stiffening alone is sufficient to increase the density of CCD-19Lu fibroblasts

We engineered culture substrata based on PAA gels to mimic normal (∼1 kPa) and desmoplastic (∼30 kPa) mechanical microenvironments (Fig. 2A), and used them to examine the relative effects of matrix stiffening and serum stimulation on cell density in CCD-19Lu fibroblasts. Although PAA gels are somewhat limited in that they provide a 2D rather than 3D microenvironment, their physiopathologic relevance has been extensively validated (22, 27, 28). After 5 days in culture, the normalized cell density (D) rose with serum concentration according to an exponential function ($r^2 > 0.99$) in both 1 kPa (dashed) and 30 kPa gels (solid line; Fig. 2B and Supplementary Material). However, cell density data were consistently higher in 30 kPa than in 1 kPa gels for all FBS (%) values. To compare quantitatively the effects of mechanical and soluble mitogenic cues, we assessed the relative fibroblast accumulation (R) by computing the percentage of increase in cell density due to matrix stiffening or serum stimulation using either the latter exponential fittings (lines) or the experimental data (white squares; Fig. 2C). The stiffening-induced fibroblast accumulation ($R_{stiffening}$) was ≥20% for all serum concentrations,

Downloaded from mcr.aacrjournals.org on September 15, 2015. © 2015 American Association for Cancer Research.

Published OnlineFirst October 3, 2014; DOI: 10.1158/1541-7786.MCR-14-0155

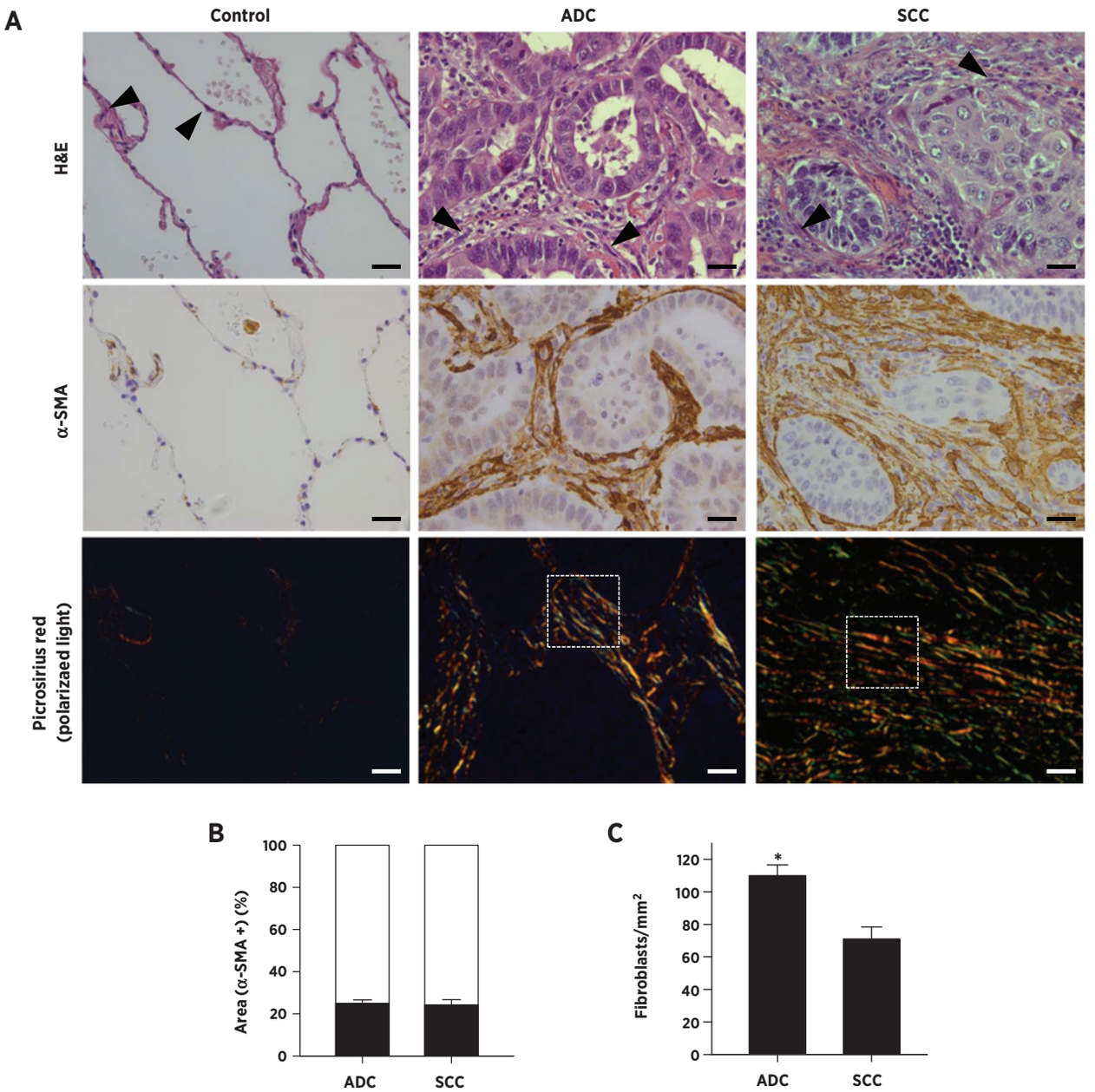


Figure 1.
The desmoplastic stroma of both ADC and SCC exhibits markers indicative of large mechanical tension compared with normal lung parenchyma. A, illustrative images of H&E (top), α-SMA (middle), and picrosirius red (bottom) stainings of histologic samples from primary control (left), ADC (middle), and SCC (right column) pulmonary tissue obtained with a ×40 objective. Arrowheads, spindle-shaped nuclei characteristic of fibroblasts. α-SMA images reveal a stroma rich in hypercontractile myofibroblasts. White dashed squares, regions with straight and parallel collagen fibers indicative of mechanical tension; scale bars, 30 μm. B, assessment of the stromal area fraction within tumor samples as the percentage of α-SMA$^+$ area in histologic sections ($n = 5$ patients/subtype). C, TAF density assessed by morphometric analysis of H&E images ($n = 10$ patients/subtype; further details in Supplementary Fig. S1–S3); *, $P \leq 0.05$ was determined by the Student t test.

including 0% FBS, and exhibited a biphasic dependence with serum that peaked at approximately 0.5% to 1% FBS. Moreover, this stiffening-induced accumulation was dominant or comparable with that due to serum (R_{serum}) up to 0.5% FBS (Fig. 2C inset and Table 1), which falls within the physiologic serum concentration for fibroblasts as reported elsewhere (29). To rule out that the large stiffening-induced accumulation in SFM was not due to the presence of insulin, cell density was measured in SFM not supplemented with ITS. In these conditions, we still observed approximately 20% accumulation in 30 kPa gels (Fig. 2D),

Downloaded from mcr.aacrjournals.org on September 15, 2015. © 2015 American Association for Cancer Research.

Published OnlineFirst October 3, 2014; DOI: 10.1158/1541-7786.MCR-14-0155

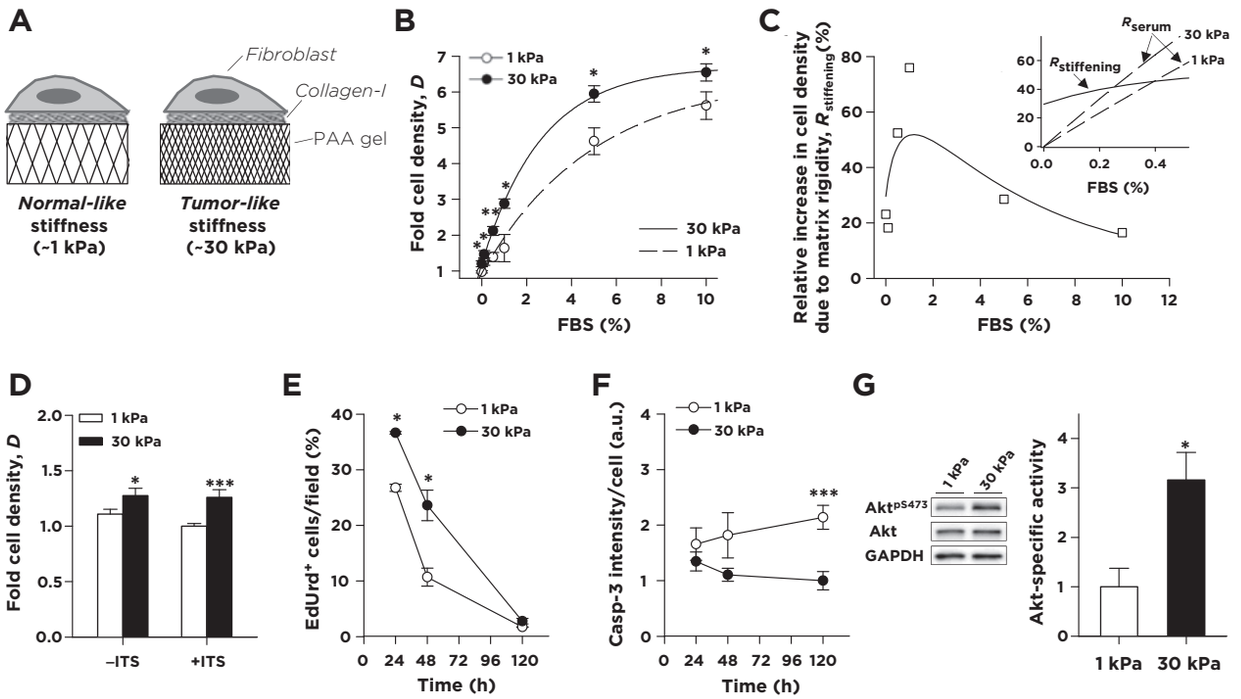


Figure 2.
Matrix rigidity enhances the accumulation of CCD19-Lu fibroblasts by ≥20% through increased proliferation and survival in SFM. A, outline of the culture assay. B, time course of normalized cell density *D* after 5 days in culture on 30 kPa (black) or 1 kPa (white dots) PAA gels in SFM supplemented with increasing serum concentrations. For each matrix rigidity, data were fitted to an exponential function (solid and dashed lines, see Supplementary Material for details). C, relative change in cell density due to matrix rigidity ($R_{stiffening}$) at different FBS(%) using either the experimental data (white squares) or the fittings in B (solid line). Inset, a comparison between the fibroblast accumulation due to either serum (R_{serum}, dashed lines) or matrix stiffening up to 0.5% FBS calculated using the fittings in B (see Table 1 for further details). D, fibroblast density at 1 and 30 kPa gels in SFM ± ITS. Unless otherwise indicated, SFM supplemented with ITS was used in all subsequent experiments. E and F, time course of the proliferative (E) and caspase-3 (F) activities. G, (left) representative Western blot analysis of $Akt^{pSer473}$, total Akt, and GAPDH in cells cultured on 1 and 30 kPa gels for 30 minutes; (right) densitometry analysis of $Akt^{pSer473}$/Akt. Unless otherwise indicated, all data here and thereafter are mean ± SE. Numerical results correspond to three replicates from at least two independent experiments; *, $P \leq 0.05$; **, $P \leq 0.01$; ***, $P \leq 0.005$ were determined by the Student *t* test comparing data at 1 and 30 kPa gels.

thereby demonstrating that matrix stiffening alone is sufficient to raise fibroblast population in the complete absence of exogenous growth factors.

Matrix stiffening drives the accumulation of CCD-19Lu fibroblasts through increased proliferation and survival in a β_1 integrin–dependent fashion

To dissect the mechanisms underlying the increased fibroblast density in 30 kPa gels, we performed a time-course analysis of proliferative and apoptotic markers in CCD-19Lu cells. The proliferative activity declined with time in both rigidities, yet it was higher at 30 kPa than at 1 kPa at all time points, with the largest difference observed at 48 hours (Fig. 2E). Conversely, caspase-3 activity was lower at 30 kPa than at 1 kPa at all times, and their difference increased over time (Fig. 2F). The increased survival cues at 30 kPa gels were confirmed independently by the early increase in Akt^{pS473} (Fig. 2G).

Because increased proliferation and decreased apoptosis have been previously associated with increased cell–ECM interactions

Table 1. Relative increase in either cell density or cells entering the cell cycle of fibroblasts stimulated with a larger matrix rigidity or FBS concentration (mean ± SE)

Stimulus A	Stimulus B	CCD-19Lu	Control fibroblasts	ADC-TAFs	SCC-TAFs
1 → 30 kPa	0% FBS	**30%**[a,d]	**41 ± 15%**[a]	**23 ± 7%**[a]	**52 ± 12%**[a]
	0.1% FBS	**35%**[a,d]	**46 ± 11%**[a]	**13 ± 2%**[a]	**54 ± 19%**[a]
0% → 0.1% FBS	1 kPa	**12%**[a,d]	**18 ± 9%**[a]	**14 ± 6%**[a]	**15 ± 2%**[a]
	30 kPa	**17%**[a,d]	**27 ± 12%**[a]	6 ± 4%[a]	11 ± 5%[a]
0% → 10% FBS	2.8×10^6 kPa[c]	123 ± 31%[b]	125 ± 34%[b]	69 ± 39%[b]	13 ± 11%[b]

NOTE: The relative increase in normalized cell density *D* due to either matrix stiffening or serum was calculated as $R_{stiffening}(\%) = 100 \times (D_{30\ kPa} - D_{1\ kPa})/D_{1\ kPa}$ and $R_{serum}(\%) = 100 \times (D_{c(\%)} - D_{0\%FBS})/D_{0\%FBS}$, respectively. The relative rise in cycling cells from 0% to 10% FBS was assessed as $R_{cycle}(\%) = 100 \times (P_{10\%FBS} - P_{0\%FBS})/P_{0\%FBS}$). It should be borne in mind that $R_{stiffening}$ and R_{serum} were measured in PAA gels, whereas R_{cycle} were measured in 2D cultures.
[a]Relative increase in cell density ($R_{stiffening}$ or R_{serum}).
[b]Relative increase in cells entering the cell cycle (R_{cycle}).
[c]Young's modulus of polystyrene used in 2D cultures (28).
[d]Values calculated with the fittings in Fig. 2C. The values in bold were statistically significant.

Downloaded from mcr.aacrjournals.org on September 15, 2015. © 2015 American Association for Cancer Research.

Published OnlineFirst October 3, 2014; DOI: 10.1158/1541-7786.MCR-14-0155

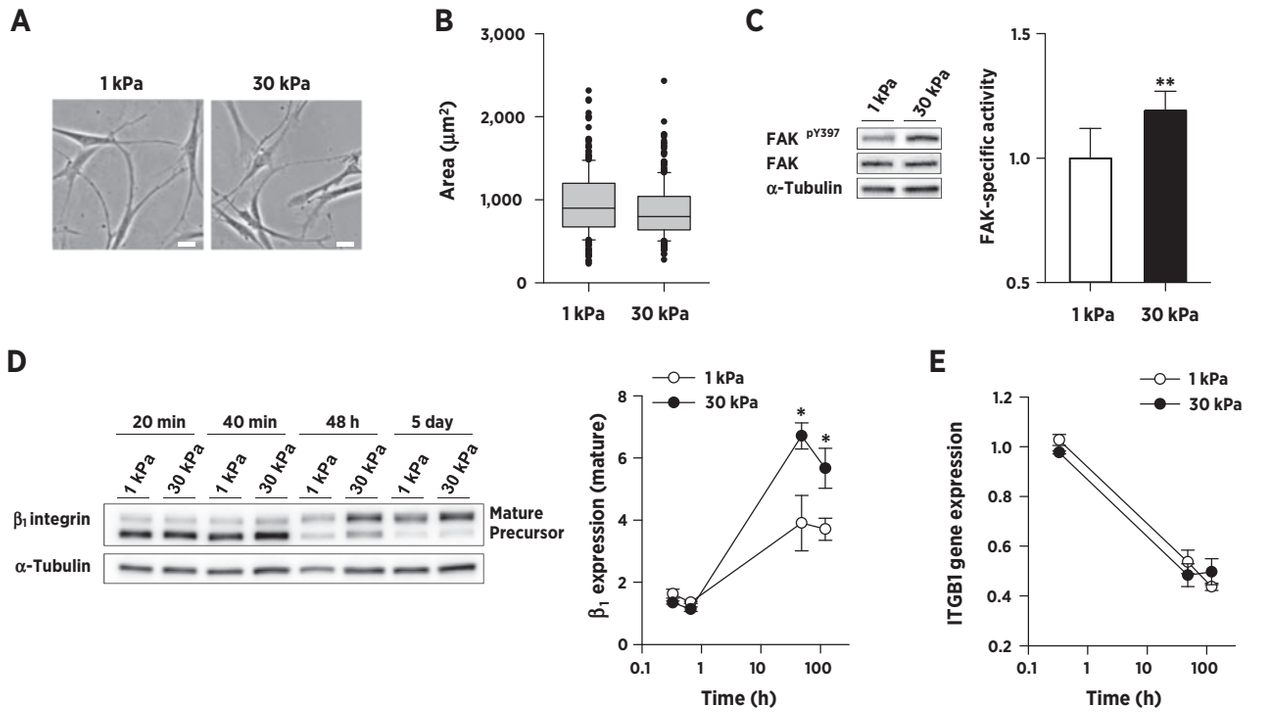


Figure 3.
Matrix rigidity induces both increased integrin mechano-sensing through FAK^{pY397} and a posttranscriptionally driven rise in β_1 integrin expression in CCD-19Lu fibroblasts. A, images of sparse fibroblasts cultured on 1 and 30 kPa PAA gels for 24 hours; scale bars, 30 μm. B, projected area of cells cultured as in A ($n > 250$ cells/condition). C, (left) representative Western blot analysis of FAK^{pY397}, total FAK, and α-tubulin in cells cultured on 1 and 30 kPa gels for 20 minutes; (right) densitometry analysis of FAK^{pY397}/FAK. D, (left) representative Western blot analysis showing the time-course expression of total β_1 integrin and loading control of cells cultured on 1 and 30 kPa gels; (right) densitometry analysis of the time-course expression of mature β_1 integrin normalized to α-tubulin. E, time course of β_1 mRNA assessed by qRT-PCR of cells cultured as in D. Numerical data correspond to three replicates from at least two independent experiments. Statistical analysis was performed as in Fig. 2 except in B, in which the Mann–Whitney rank-sum test was used.

through enhanced cell spreading (12, 30), we measured cell spreading in CCD-19Lu fibroblasts. We observed elongated and spindle-like morphologies in both 1 and 30 kPa gels (Fig. 3A). Likewise, the distribution of cell area values were comparable in both stiffness conditions (Fig. 3B), further indicating that the rise in stiffening-induced fibroblast accumulation was not due to changes in cell spreading.

Adherent cells probe the mechanochemical properties of their surrounding ECM largely through the integrin family of α/β heterodimeric ECM mechano receptors (22, 23). Accordingly, we examined whether matrix rigidity altered integrin mechano sensing by checking FAK^{pY397}, which is indicative of integrin activation and clustering, and is required for focal adhesion formation and/or stabilization in fibroblasts and other adherent cells (16, 27). We observed an early upregulation in FAK^{pY397} at 30 kPa compared with 1 kPa (Fig. 3C). Because fibroblasts were seeded on collagen-I–coated gels, we examined the specific involvement of integrin collagen-I receptors. In fibroblasts, these receptors include three integrins that share the β_1 subunit ($\alpha_1\beta_1$, $\alpha_2\beta_1$, and $\alpha_{11}\beta_1$; refs. 31, 32). Accordingly, we first conducted a time-course analysis of β_1 integrin expression by Western blotting (Fig. 3D and E). Protein levels of mature β_1 integrin were comparable at short times (≤1 hour) in both stiffnesses (Fig. 3D), indicating that the difference in FAK^{pY397} between matrix rigidities was due to increased β_1 integrin mechano-sensing rather than to altered expression. β_1 integrin levels increased at longer times (>>1 hour) in all rigidity conditions, but this increase was more pronounced at 30 kPa (~6-fold) than at 1 kPa (~3-fold), with the largest difference observed at 48 hours. To shed light on the mechanisms underlying this protein dynamics, we performed a time-course analysis of β_1 integrin mRNA (Fig. 3E). Unlike the protein level, no significant differences were found between the mRNA obtained in both stiffness conditions at all time points. Likewise, a similar ratio between mature (i.e., fully glycosylated) and precursor (i.e., partially glycosylated) β_1 integrins was observed in 1 and 30 kPa gels up to 48 hours (Supplementary Fig. S5), indicating that the rise in mature β_1 integrin observed at 48 hours was not due to transcriptional regulation, but rather to posttranscriptional processes other than enhanced glycosylation.

To check whether β_1 integrins were necessary for the larger cell density observed in 30 kPa gels, we treated CCD-19Lu fibroblasts with increasing concentrations (c_{inh}) of the β_1 integrin inhibitory antibody AIIB2 (16, 33). We observed a dose-dependent decrease in cell density in cells cultured in 30 kPa gels treated with AIIB2 but not with IgG1. Such decrease was well captured by an exponential decay (solid line), eliciting $c_{inh,50} = 3.8$ μg/mL (Fig. 4A). Fibroblasts cultured on 30 kPa gels treated with 3 μg/mL AIIB2—close to $c_{inh,50}$—downregulated both FAK^{pY397} (Fig. 4B) and mature β_1 integrin expression (Fig. 4C) to levels comparable with those observed at 1 kPa. Likewise, AIIB2 downregulated the proliferative

Downloaded from mcr.aacrjournals.org on September 15, 2015. © 2015 American Association for Cancer Research.

Published OnlineFirst October 3, 2014; DOI: 10.1158/1541-7786.MCR-14-0155

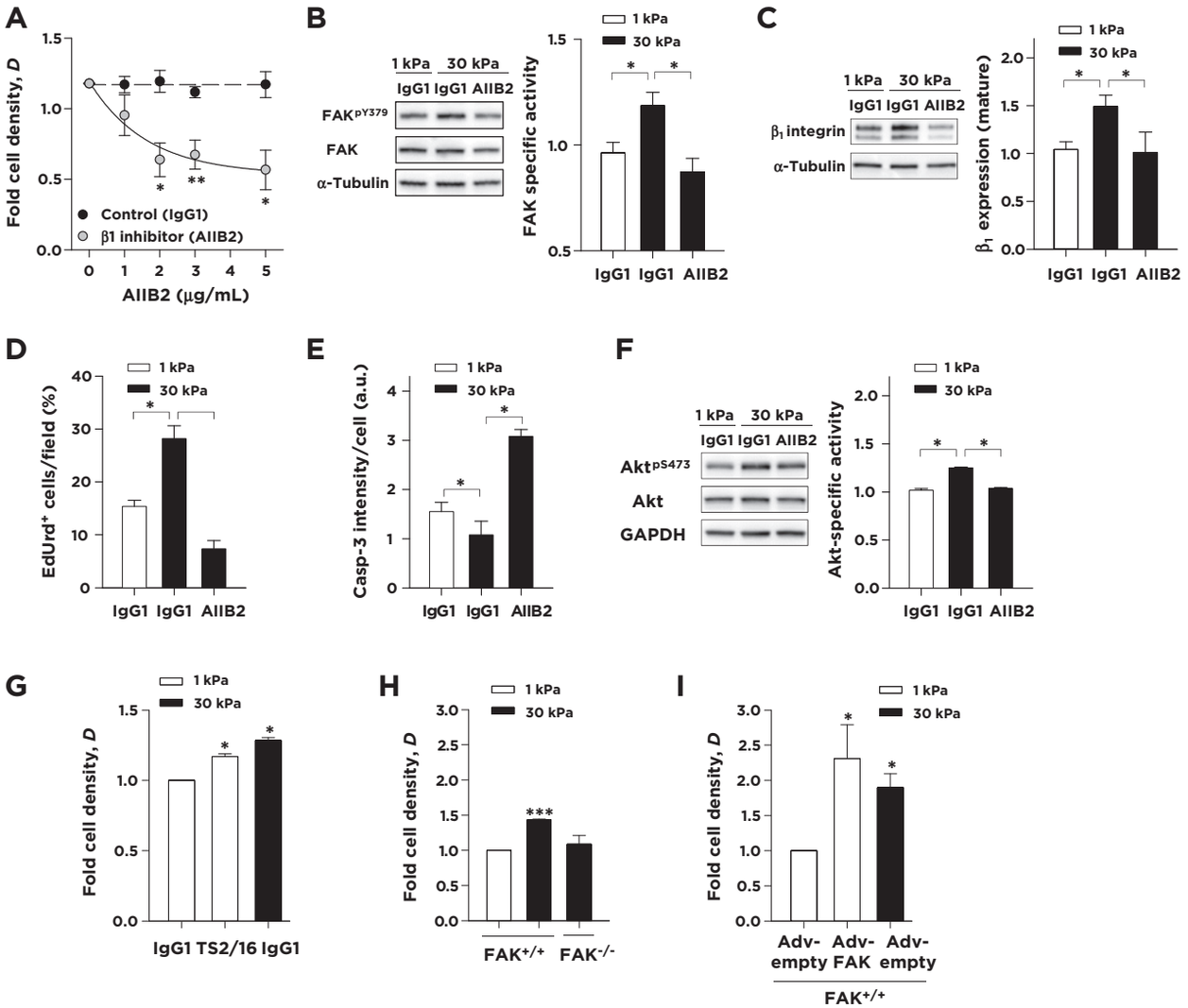


Figure 4.

Inhibition of β_1 integrin or FAK depletion prevent matrix rigidity-induced accumulation of fibroblasts in 30 kPa gels, whereas forcing β1 integrin activation or FAK expression act otherwise. A, dose–response effects of β_1 integrin inhibitory antibody AIIB2 and control IgG1 antibody on the density of CCD-19Lu cells cultured for 5 days on 30 kPa gels. Solid and dashed lines correspond to a fitting to an exponential function and to the average of AIIB2 and IgG1 data, respectively (see Supplementary Material for details). B, (left) representative Western blot analysis of FAK^{pY397}, total FAK, and α-tubulin (left) in CCD-19Lu cells cultured on either 1 kPa gels and treated with IgG1 or on 30 kPa gels and treated with 3 μg/mL IgG1 or AIIB2; (right) densitometry analysis of FAK^{pY397}/FAK. C, (left) representative Western blot analysis of total β_1 and α-tubulin in cells cultured as in B for 48 hours; (right) densitometry analysis of mature β_1. D and E, proliferative (D) and apoptotic (E) activities of CCD-19Lu cells cultured as in B for 48 hours and 5 days, respectively, assessed as in Fig. 2. F, (left) representative Western blot analysis of $Akt^{pSer473}$, total Akt, and GAPDH (left) of cells cultured as in B; (right) densitometry analysis of $Akt^{pSer473}$/Akt. G, normalized cell density of CCD-19Lu fibroblasts treated with TS2/16 β_1 integrin–activating or control (IgG1) antibodies. H, normalized cell density of FAK wild-type ($FAK^{+/+}$) and FAK-null ($FAK^{-/-}$) mouse MEFs. I, normalized cell density of FAK-overexpressing (Adv-FAK) and control (Adv-empty) wild-type MEFs. Numerical results correspond to three replicates from at least two independent experiments. Statistical analysis was performed as in Fig. 2 by comparing each group with respect to either IgG1 at 30 kPa (A–G) or control conditions at 1 kPa (H and I). *, $P < 0.05$; **, $P < 0.01$; ***, $P < 0.005$.

activity (Fig. 4D), whereas it upregulated cleaved caspase-3 (Fig. 4E) and reduced Akt^{pS473} (Fig. 4F) to levels similar to those observed at 1 kPa. On the other hand, activating β_1 integrin with 5 μg/mL TS2/16 antibody—which binds β_1 integrin within the same small region than AIIB2 (34)—was sufficient to increase both cell density (Fig. 4G) and FAK^{pY397} expression of CCD-19Lu fibroblasts in 1 kPa gels compared with IgG1 treatment (Supplementary Fig. S6). To confirm further the requirement of β_1 integrin mechano-sensing through FAK^{pY397} in matrix stiffening–driven fibroblast accumulation, we either depleted or overexpressed FAK in MEFs as previously described (24). As in CCD-19 Lu fibroblasts, matrix stiffening enhanced cell density and FAK^{pY397} expression in wild-type MEFs ($FAK^{+/+}$), whereas such increases were not observed in FAK null fibroblasts ($FAK^{-/-}$; Fig. 4H and Supplementary Fig. S6). Conversely, overexpressing FAK in wild-type MEFs was sufficient to markedly increase both cell density (Fig. 4I)

Downloaded from mcr.aacrjournals.org on September 15, 2015. © 2015 American Association for Cancer Research.

Published OnlineFirst October 3, 2014; DOI: 10.1158/1541-7786.MCR-14-0155

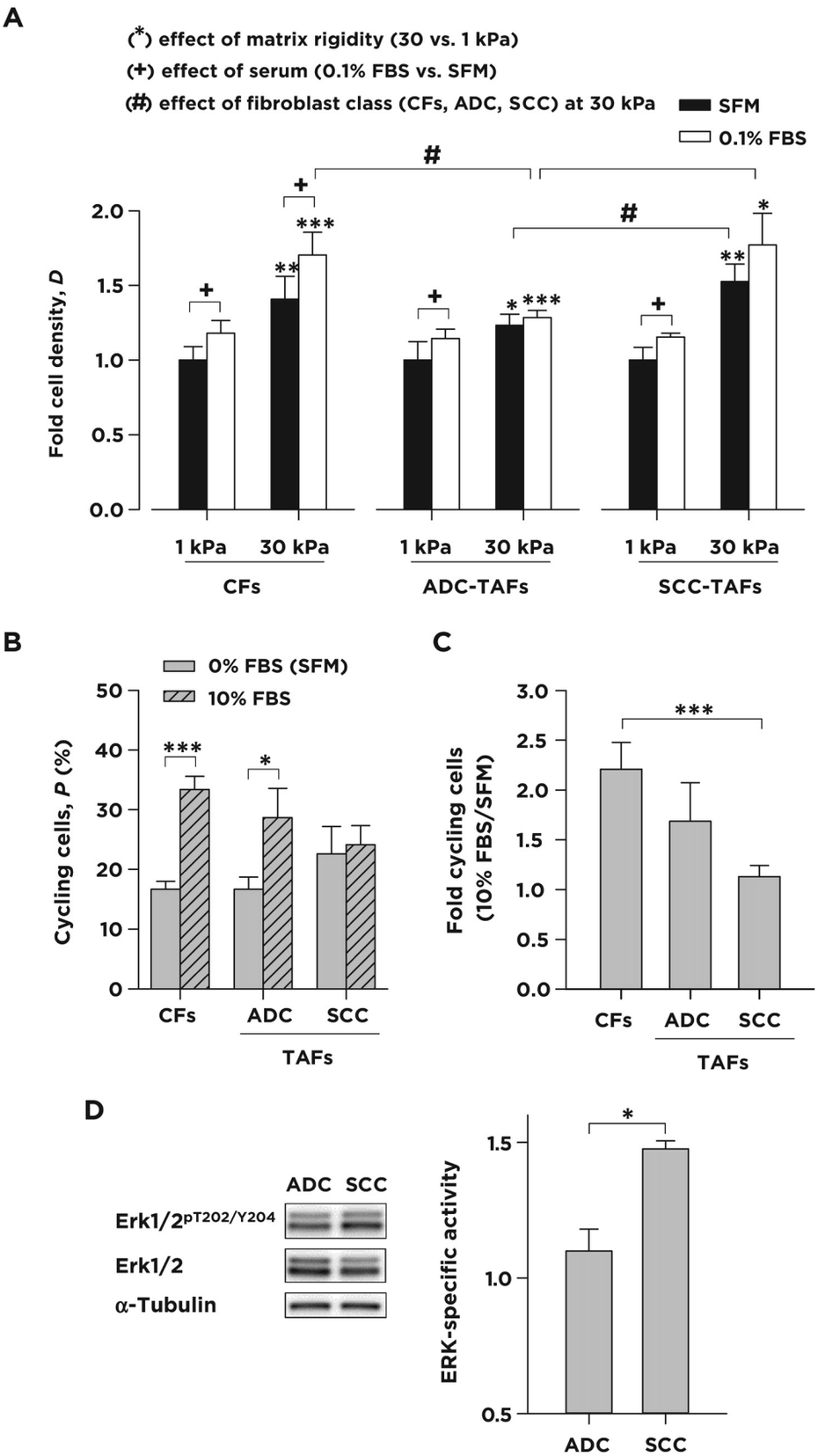


Figure 5.
Primary TAFs exhibit subtype-specific aberrant responses to either matrix rigidity or serum with respect to primary control fibroblasts. A, normalized cell density in three classes of primary fibroblasts (control fibroblasts, ADC–TAFs, and SCC–TAFs) cultured as in Fig. 2 in SFM or 0.1% FBS. Two-group comparisons within classes were performed to analyze the effect of either matrix rigidity (*) or serum (+). Statistical analyses between classes (#) were restricted to 30 kPa gels ($n = 10$ for control fibroblasts; $n = 5$ for both ADC–TAFs, and SCC–TAFs). All P values are shown in Supplementary Table S2. B, the percentage of cycling fibroblasts (i.e., in S and G_2–M) cultured in 2D in SFM or 10% FBS for 5 days ($n = 10$ for control fibroblasts; $n = 6$ for both ADC–TAFs, and SCC–TAFs). C, the ratio between percentages at 10% FBS and SFM. D, (left) representative Western blot analysis of Erk1/2$^{pT202/Y204}$, total Erk1/2, and loading of TAFs cultured in 2D for 20 minutes; (right) densitometry analysis of Erk1/2$^{pT202/Y204}$/Erk1/2 ($n = 3$/subtype). *, $P < 0.05$; **, $P < 0.01$; ***, $P < 0.005$.

Downloaded from mcr.aacrjournals.org on September 15, 2015. © 2015 American Association for Cancer Research.

Published OnlineFirst October 3, 2014; DOI: 10.1158/1541-7786.MCR-14-0155

and FAK^{pY397} expression (Supplementary Fig. S6) in 1 kPa gels compared with control MEFs.

The accumulation of primary SCC–TAFs in culture requires matrix stiffening, whereas that of ADC–TAFs demands high serum concentration

To examine whether the findings obtained with CCD-19Lu cells and MEFs could be extended to primary fibroblasts, we assessed the fibroblast accumulation due to either matrix stiffening or 0.1% FBS in primary NSCLC–TAFs and corresponding control fibroblasts. As in CCD-19Lu cells and MEFs, cell density in control fibroblasts was consistently higher in 30 kPa than in 1 kPa gels (Fig. 5A), and this difference was associated with increased proliferative and decreased apoptotic activities (Supplementary Fig. S7). Likewise, matrix stiffening-induced accumulation increased in TAFs, yet in a subtype-specific fashion according to SCC (>50%) > ADC (∼10%–20%; Table 1). In further agreement with CCD-19Lu cells, the relative accumulation due to matrix stiffening was consistently larger than that due to 0.1% FBS in primary fibroblasts (Table 1). Intriguingly, the serum-dependent accumulation at 30 kPa gels was much lower in TAFs than in control fibroblasts or CCD-19Lu fibroblasts, particularly in ADC–TAFs. To check whether the latter poor serum responses were due to an impairment in cell-cycle progression, we examined the ability of TAFs cultured in 2D to enter the cell cycle in response to 10% FBS by flow cytometry (Fig. 5B). The percentage of cycling cells (i.e., cells that entered into either S or G_2–M) at 10% FBS with respect to 0% FBS almost doubled in both control fibroblasts and ADC–TAFs, whereas it remained unaltered in SCC–TAFs (Fig. 5C). Indeed, the relative rise in cycling cells from 0% to 10% FBS was comparable with the relative accumulation of fibroblasts induced by 0.1% FBS in SCC–TAFs (Table 1), revealing a very weak serum response in this subtype. Of note, the percentage of cycling cells at 0% FBS in SCC–TAFs was 35% larger than that in control fibroblasts or ADC–TAFs (Fig. 5B), suggesting an intrinsic overactivation of mitogenic activity in the absence of exogenous growth factors in SCC–TAFS. In support of the latter interpretation, we observed higher Erk1/2$^{pT202/Y204}$ in SCC–TAFs compared with ADC–TAFs in 2D (Fig. 5D). To our knowledge, these results report for the first time subtype-specific responses to extracellular mechanical and soluble mitogenic cues in TAFs.

β_1 integrin protein levels *in vivo* and in culture correlate with the relative increase in primary TAF accumulation in stiff substrata

The relative differences in cell density among primary TAFs and control fibroblasts observed in 30 kPa gels (Fig. 5A) were reproduced in 2D cultures (Fig. 6A and Supplementary Fig. S8). These observations are in accordance with previous studies reporting that cell behavior in 2D cultures is qualitatively similar to that observed in stiff PAA gels, whereas it enhances quantitatively the trends observed from soft to stiff PAA gels (11, 27). Accordingly, we used 2D cultures to gain molecular insights underlying the differences between ADC–TAFs and SCC–TAFs in stiff microenvironments. We observed higher proliferative activity in SCC–TAFs than in ADC–TAFs in 2D (Fig. 6B), whereas caspase-3 activity (Fig. 6C) and Akt^{pS473} levels (Fig. 6D) remained comparable in both subtypes. These results are consistent with the larger percentage of cycling cells and Erk1/2$^{pT202/Y204}$ observed in SCC–TAFs than in ADC–TAFs at 0% FBS, and suggest that the enhanced matrix stiffening-induced accumulation in SCC–TAFs was driven by increased proliferative rather than survival cues. In addition, we found that both FAK^{pY397} (Fig. 6E) and β_1 expression (Fig. 6F) followed the same trend in 2D than that of the matrix stiffening increased fibroblast accumulation (i.e., SCC > ADC). Moreover, the differences in cell density between ADC–TAFs and SCC–TAFs were abrogated upon treatment with 3 μg/mL AIIB2 (Fig. 6G). These results confirmed that matrix stiffening-driven fibroblast accumulation was β_1 integrin dependent in TAFs, and revealed that the higher accumulation observed in SCC–TAFs compared with ADC–TAFs in 30 kPa gels was associated with larger β_1 integrin expression and mechano-sensing through FAK^{pY397}. In agreement with the latter association, overexpressing FAK in wild-type MEFs cultured in 30 kPa gels was sufficient to increase cell density by approximately 40% with respect to control MEFs (Supplementary Fig. S9). To extend these observations to the tissue context, we examined β_1 integrin in TAFs *in vivo* by immunohistochemistry. In agreement with our culture data, image analysis revealed a higher percentage of stromal cells with strong β_1 integrin staining in SCC (50% ± 6%) than in ADC (36% ± 2%, $P = 0.03$) tumor samples (Fig. 6H and Supplementary Fig. S10).

Discussion

The cancer subtype specificity of stromal desmoplastic features remains ill defined in NSCLC. We found that TAFs were overwhelmingly α-SMA$^+$ and peritumoral in both ADC and SCC subtypes of NSCLC, thereby extending previous observations on lung ADC (15, 35). We also reported for the first time that the desmoplastic stroma accounts for approximately 25% of the total tumor in both subtypes. Likewise, we observed two collagen signatures previously associated with matrix stiffening in both subtypes: An increased collagen amount and peritumoral stretched collagen fibers (36). Intriguingly, despite these similar desmoplastic features, we found a markedly distinct TAF density between ADC and SCC *in vivo*, which suggests that TAF accumulation may be driven through subtype-specific mechanisms.

To dissect the functional role of matrix stiffening in NSCLC stromagenesis, we first compared the relative contribution of matrix rigidity and soluble mitogenic factors in the accumulation of lung fibroblasts from nonmalignant tissue. We showed for the first time that matrix stiffening alone was sufficient to drive fibroblast accumulation by ≥20%, even in the absence of exogenous growth factors. Moreover, the effect of matrix stiffening on fibroblast density was dominant or comparable with that due to mitogenic cues present in serum up to 0.5% FBS, which is a more physiologic concentration than the 10% to 20% FBS used in many cell culture studies. All these findings strongly support that matrix stiffening alone may be as important as soluble growth factors in driving fibroblast accumulation *in vivo*, thereby challenging the current view of stromagenesis as driven by paracrine signaling only (3, 8–10). Moreover, they extend previous evidence of a positive feedback loop in which activated fibroblasts lay out increased amounts of fibrotic ECM components that render a stiffer ECM, which in turn may drive fibroblast activation and accumulation further (11, 14).

The mechanisms by which matrix stiffening enhances fibroblast density had remained elusive. In fibroblasts from nonmalignant tissue, we demonstrated that mechanically driven

Downloaded from mcr.aacrjournals.org on September 15, 2015. © 2015 American Association for Cancer Research.

Published OnlineFirst October 3, 2014; DOI: 10.1158/1541-7786.MCR-14-0155

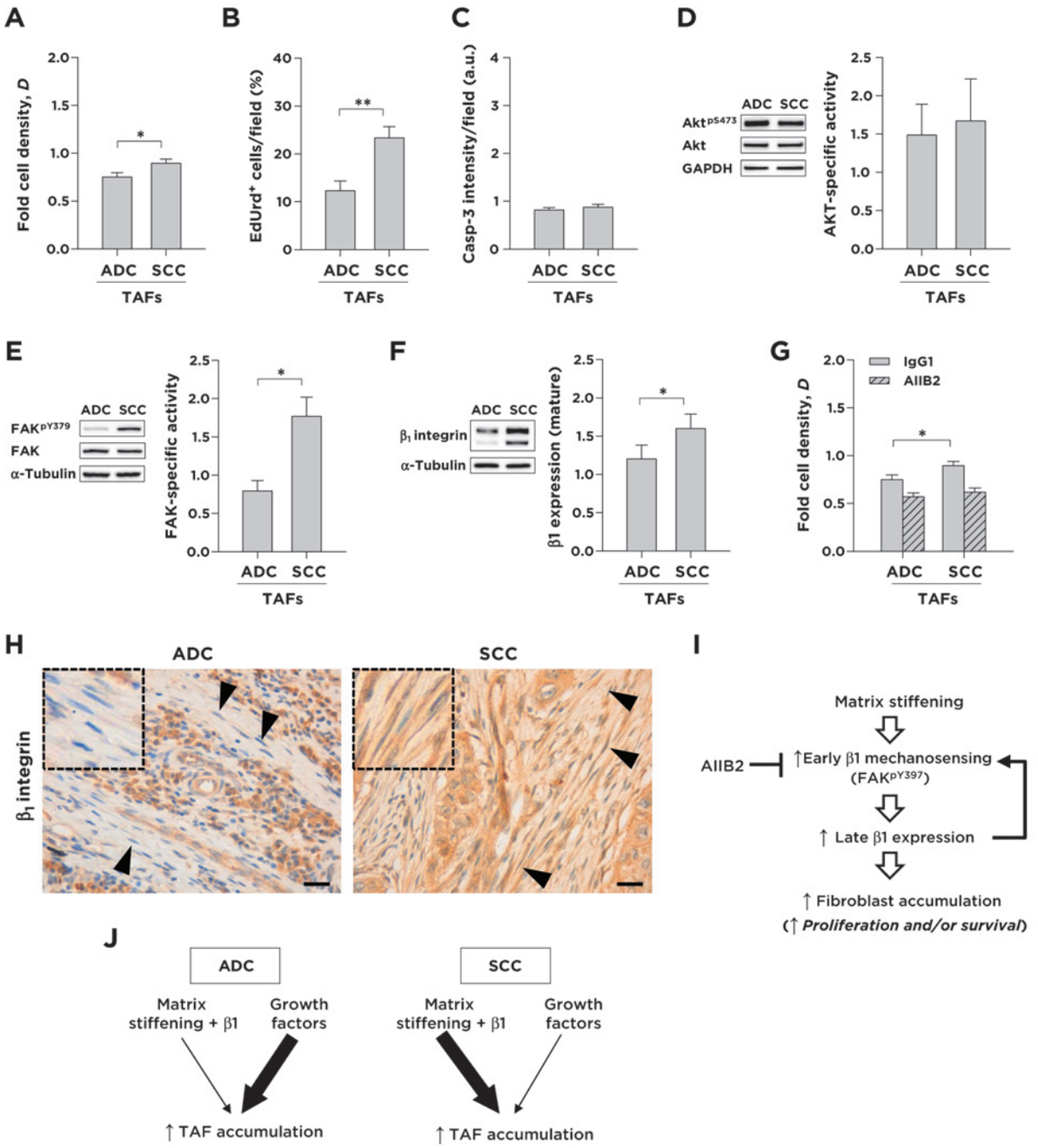


Figure 6.
The larger cell accumulation, proliferative activity, integrin mechano-sensing, and β_1 expression in SCC–TAFs with respect to ADC–TAFs in 2D culture are associated with higher β_1 expression of SCC–TAFs *in vivo*. A to D, normalized fibroblast density ($n = 9$; A), proliferation ($n = 6$; B), apoptosis ($n = 6$; C), and survival signaling ($n = 3$; D) of TAFs in 2D culture. E and F, representative Western blots and average densitometry analyses of FAK ($n = 3$; E) and β_1 integrin ($n = 9$; F) of TAFs in 2D culture. Assays in A to F performed as in Fig. 4. G, normalized density of TAFs in 2D culture treated with 3 μg/mL IgG1 or AIIB2 ($n = 9$ and 6, respectively). H, (left) illustrative images of histologic β_1 integrin stainings obtained with a ×40 objective. Arrowheads, to fibroblasts. Insets, enlarged fibroblast-rich regions within each image; scale bars, 30 μm. Additional examples and full scoring details are given in Supplementary Fig. S10. I, outline of the emerging mechano-regulatory mechanism of fibroblast accumulation. J, scheme illustrating the differential regulation of mechanical and soluble mitogenic cues in ADC–TAFs and SCC–TAFs. *, $P < 0.05$; **, $P < 0.01$; ***, $P < 0.005$.

cell accumulation requires β_1 integrin receptors. Moreover, matrix stiffening induced an early increase in β_1 integrin mechano-sensing through FAK^{pY397} followed by a rise in Akt^{pS473}, which were associated with increased proliferative and survival activities. Further evidence for a mechanistic relationship between β_1, FAK^{pY397} and Akt^{pS473} has been

Downloaded from mcr.aacrjournals.org on September 15, 2015. © 2015 American Association for Cancer Research.

Published OnlineFirst October 3, 2014; DOI: 10.1158/1541-7786.MCR-14-0155

previously reported in fibroblasts and epithelial cells in response to distinct mechanical stimuli in the presence of growth factors (16, 37, 38). In contrast, we show that exogenous growth factors are not required to activate this regulatory mechanism. In addition, matrix stiffening increased mature β_1 integrin levels at a later time scale (>>1 h) at the protein but not mRNA levels. Conversely, the mechanically driven increases in early FAK^{pY397} and late posttranscriptional β_1 integrin were abrogated with a β_1 integrin inhibitor, whereas FAK^{pY397} was enhanced with a β_1 integrin–activating antibody, thereby strongly suggesting a common regulatory process. The latter interpretation was validated independently by genetic manipulations in fibroblasts in which FAK was either depleted or overexpressed. To our knowledge, these are the first observations that posttranscriptional integrin regulation can be driven by matrix rigidity in fibroblasts. Unraveling the molecular complexity underlying such posttranscriptional regulation (39, 40) will require future investigations. However, whatever the regulatory mechanism might be, it is conceivable that the functional role of the enhanced β_1 integrin level is to reinforce the $\beta_1/FAK^{pY397}/Akt^{pS473}$ mechano-regulatory pathway to further stabilize focal adhesions and fibroblast accumulation as outlined in Fig. 6I.

The mechano-regulatory mechanism observed in fibroblasts from nonmalignant tissue could be somewhat extended to TAFs (Fig. 6I), because matrix stiffening increased TAF accumulation through β_1 integrins. However, some aspects of this mechano-regulatory pathway were different in control fibroblasts than in TAFs in a subtype-specific fashion. Thus, mechanically induced fibroblast accumulation was larger in SCC–TAFs and lower in ADC–TAFs than control fibroblasts and CCD-19Lu cells (Table 1). Likewise, we reported the novel observation of a higher β_1 integrin expression in SCC–TAFs than in ADC–TAFs both in culture and *in vivo*. In agreement with this finding, a larger expression of the alpha subunits of collagen-I integrin receptors in fibroblasts (31, 32) has been reported in SCC compared with ADC (41). The mechanisms underlying the larger β_1 integrin expression in SCC–TAFs remain unknown. However, it is possible that the integrin regulator kindlin-2—a focal adhesion protein involved in integrin activation through interactions with the β subunit—may be involved, according to a recently reported lower stromal kindlin-2 expression in SCC compared with ADC (42).

We reported another novel subtype-specific difference in TAFs in terms of serum response. Unlike control fibroblasts, the accumulation of ADC–TAFs in culture required high serum concentration, whereas matrix stiffening effects were weak. In contrast, SCC–TAFs were largely serum desensitized, revealing that their accumulation required a stiff microenvironment (Fig. 6J). This serum desensitization was associated with a larger Erk1/2 activation, mitogenic activity, and β_1 integrin expression in SCC–TAFs compared with ADC–TAFs in SFM, which are consistent with the crosstalk between integrins and growth factor receptor signaling reported elsewhere (43). The mechanisms underlying the distinct molecular features observed in ADC–TAFs and SCC–TAFs remain unknown. However, they could be associated with differences in the secretome of cancer cells from these two subtypes (44). Unlike stiff substrata, no marked differences in absolute (not normalized) cell density values were observed in 1 kPa gels between ADC–TAFs and SCC–TAFs (Supplementary Fig. S11), supporting that the subtype-specific differences in TAF accumulation require both extrinsic (i.e., matrix stiffening) and intrinsic (β1 integrin, Erk1/2 activity) cues. Taken altogether, these observations challenge further the common assumption that all tumor desmoplastic stromas arise through similar processes akin to generic wound repair (4, 7).

The current paradigm of TAF accumulation based on repair-like processes (3, 8–10) supports a therapeutic strategy to reduce their density based on inhibiting stromal growth factors. Our data support the latter strategy in ADC–TAFs but not in SCC–TAFs. In agreement with this hypothesis, an inhibitor of multiple tyrosine kinases—many of which are known promitogenic effectors in fibroblasts—in combination with docetaxel has been recently reported to be therapeutically effective in patients with NSCLC with advanced ADC but not with SCC subtpype (45). In contrast, our results support a novel strategy to target SCC–TAFs based on either restoring normal lung elasticity and/or β_1 integrin–dependent mechano regulation. This new approach may be particularly clinically relevant according to a recent report that SCC samples exhibit an intratumoral pressure approximately 25% greater than ADC (46). Of note, successful therapeutic approaches aiming to rescue normal tissue mechano regulation have been recently reported in animal models of fibrosis and cancer (16, 47, 48), raising the exciting possibility that these or related approaches may be effective against SCC NSCLC.

Disclosure of Potential Conflicts of Interest

No potential conflicts of interest were disclosed.

Authors' Contributions

Conception and design: M. Puig, N. Reguart, J. Alcaraz
Development of methodology: M. Puig, R. Lugo, M. Gabasa, A. Giménez, J. Ramírez, F. Rodríguez-Pascual, N. Reguart, J. Alcaraz
Acquisition of data (provided animals, acquired and managed patients, provided facilities, etc.): M. Puig, R. Lugo, M. Gabasa, A. Velásquez, R. Galgoczy, A. Gómez-Caro, F. Rodríguez-Pascual, N. Reguart, J. Alcaraz
Analysis and interpretation of data (e.g., statistical analysis, biostatistics, computational analysis): M. Puig, R. Lugo, M. Gabasa, A. Velásquez, R. Galgoczy, J. Ramírez, P. Gascón, N. Reguart, J. Alcaraz
Writing, review, and/or revision of the manuscript: M. Puig, J. Ramírez, A. Gómez-Caro, F. Rodríguez-Pascual, P. Gascón, N. Reguart, J. Alcaraz
Administrative, technical, or material support (i.e., reporting or organizing data, constructing databases): M. Puig, Ó. Busnadiego, N. Reguart
Study supervision: M. Puig, R. Lugo, J. Ramírez, P. Gascón, N. Reguart, J. Alcaraz

Acknowledgments

The authors thank Rocío Nieto, Maeba Polo, Víctor Peinado (UB), and the Citomics and Biobank Units (IDIBAPS) for technical assistance, and Paraic Kenny (AECM), Daniel Navajas and Ramon Farré (UB) for support.

Grant Support

This work was supported by grants from the Ministerio de Economía y Competitividad (SAF2009-13243 and PI13/02368, to J. Alcaraz; PS09/01377, to N. Reguart; SAF2012-34916, to F. Rodríguez-Pascual), AECC (10/103; to N. Reguart and J. Alcaraz), SEPAR (2009-853; to N. Reguart), and predoctoral fellowships from the Fundació Cellex (to M. Puig), Ministerio de Educación (to A. Giménez), CONACYT (to R. Lugo), and COLCIENCIAS (to A. Velásquez).

The costs of publication of this article were defrayed in part by the payment of page charges. This article must therefore be hereby marked *advertisement* in accordance with 18 U.S.C. Section 1734 solely to indicate this fact.

Received March 20, 2014; revised September 4, 2014; accepted September 22, 2014; published OnlineFirst October 3, 2014.

Downloaded from mcr.aacrjournals.org on September 15, 2015. © 2015 American Association for Cancer Research.

Published OnlineFirst October 3, 2014; DOI: 10.1158/1541-7786.MCR-14-0155

References

1. Larsen JE, Minna JD. Molecular biology of lung cancer: clinical implications. Clin Chest Med 2011;32:703–40.
2. Bissell MJ, Hines WC. Why don't we get more cancer? A proposed role of the microenvironment in restraining cancer progression. Nat Med 2012;17:320–9.
3. Bhowmick NA, Neilson EG, Moses HL. Stromal fibroblasts in cancer initiation and progression. Nature 2004;432:332–7.
4. Dvorak HF, Flier J, Frank H. Tumors—wounds that do not heal—similarities between tumor stroma generation and wound-healing. N Engl J Med 1986;315:1650–9.
5. Mueller MM, Fusenig NE. Friends or foes—bipolar effects of the tumour stroma in cancer. Nat Rev Cancer 2004;4:839–49.
6. Beacham DA, Cukierman E. Stromagenesis: the changing face of fibroblastic microenvironments during tumor progression. Semin Cancer Biol 2005;15:329–41.
7. Tuxhorn JA, Ayala GE, Smith MJ, Smith VC, Dang TD, Rowley DR. Reactive stroma in human prostate cancer: induction of myofibroblast phenotype and extracellular matrix remodeling. Clin Cancer Res 2002;8:2912–23.
8. Kis K, Liu X, Hagood JS. Myofibroblast differentiation and survival in fibrotic disease. Expert Rev Mol Med 2011;13:e27.
9. Bremnes RM, Donnem T, Al-Saad S, Al-Shibli K, Andersen S, Sirera R, et al. The role of tumor stroma in cancer progression and prognosis emphasis on carcinoma-associated fibroblasts and non–small cell lung cancer. J Thorac Oncol 2011;6:209–17.
10. Singer AJ, Clark RA. Cutaneous wound healing. N Engl J Med 1999;341:738–46.
11. Liu F, Mih JD, Shea BS, Kho AT, Sharif AS, Tager AM, et al. Feedback amplification of fibrosis through matrix stiffening and COX-2 suppression. J Cell Biol 2010;190:693–706.
12. Wang HB, Dembo M, Wang YL. Substrate flexibility regulates growth and apoptosis of normal but not transformed cells. Am J Physiol-Cell Physiol 2000;279:C1345–C50.
13. Grinnell F, Zhu MF, Carlson MA, Abrams JM. Release of mechanical tension triggers apoptosis of human fibroblasts in a model of regressing granulation tissue. Exp Cell Res 1999;248:608–19.
14. Alcaraz J, Mori H, Ghajar CM, Brownfield D, Galgoczy R, Bissell MJ. Collective epithelial cell invasion overcomes mechanical barriers of collagenous extracellular matrix by a narrow tube-like geometry and MMP14-dependent local softening. Integr Biol 2011;3:1153–66.
15. Navab R, Strumpf D, Bandarchi B, Zhu CQ, Pintilie M, Ramnarine VR, et al. Prognostic gene-expression signature of carcinoma-associated fibroblasts in non–small cell lung cancer. Proc Natl Acad Sci U S A 2011;108:7160–5.
16. Levental KR, Yu H, Kass L, Lakins JN, Egeblad M, Erler JT, et al. Matrix crosslinking forces tumor progression by enhancing integrin signaling. Cell 2009;139:891–906.
17. Plodinec M, Loparic M, Monnier CA, Obermann EC, Zanetti-Dallenbach R, Oertle P, et al. The nanomechanical signature of breast cancer. Nat Nanotechnol 2012;7:757–65.
18. Gabasa M, Royo D, Molina-Molina M, Roca-Ferrer J, Pujols L, Picado C, et al. Lung myofibroblasts are characterized by down-regulated cyclooxygenase-2 and its main metabolite, prostaglandin E2. PLoS ONE 2013;8:e65445.
19. Abramoff MD, Magelhaes PJ, Ram SJ. Image processing with ImageJ. Biophotonics Int 2004;11:36–42.
20. Hartel M, di Mola FF, Gardini A, Zimmermann A, Di Sebastiano P, Guweidhi A, et al. Desmoplastic reaction influences pancreatic cancer growth behavior. World J Surg 2004;28:818–25.
21. Marin-Corral J, Fontes CC, Pascual-Guardia S, Sanchez F, Olivan M, Argiles JM, et al. Redox balance and carbonylated proteins in limb and heart muscles of cachectic rats. Antioxid Redox Signal 2010;12:365–80.
22. Alcaraz J, Xu R, Mori H, Nelson CM, Mroue R, Spencer VA, et al. Laminin and biomimetic extracellular elasticity enhance functional differentiation in mammary epithelia. EMBO J 2008;27:2829–38.
23. Acerbi I, Luque T, Gimenez A, Puig M, Reguart N, Farre R, et al. Integrin-specific mechanoresponses to compression and extension probed by cylindrical flat-ended AFM tips in lung cells. PLoS ONE 2012;7:e32261.
24. Lagares D, Busnadiego O, Garcia-Fernandez RA, Kapoor M, Liu S, Carter DE, et al. Inhibition of focal adhesion kinase prevents experimental lung fibrosis and myofibroblast formation. Arthritis Rheum 2012;64:1653–64.
25. Nunez R. DNA measurement and cell cycle analysis by flow cytometry. Curr Issues Mol Biol 2001;3:67–70.
26. Haviv I, Polyak K, Qiu W, Hu M, Campbell I. Origin of carcinoma associated fibroblasts. Cell Cycle 2009;8:589–95.
27. Paszek MJ, Zahir N, Johnson KR, Lakins JN, Rozenberg GI, Gefen A, et al. Tensional homeostasis and the malignant phenotype. Cancer Cell 2005;8:241–54.
28. Engler AJ, Sen S, Sweeney HL, Discher DE. Matrix elasticity directs stem cell lineage specification. Cell 2006;126:677–89.
29. Schwarz R, Colarusso L, Doty P. Maintenance of differentiation in primary cultures of avian tendon cells. Exp Cell Res 1976;102:63–71.
30. Roca-Cusachs P, Alcaraz J, Sunyer R, Samitier J, Farre R, Navajas D. Micropatterning of single endothelial cell shape reveals a tight coupling between nuclear volume in G_1 and proliferation. Biophys J 2008;94:4984–95.
31. Egeblad M, Rasch MG, Weaver VM. Dynamic interplay between the collagen scaffold and tumor evolution. Curr Opin Cell Biol 2010;22:697–706.
32. Eckes B, Zweers MC, Zhang ZG, Hallinger R, Mauch C, Aumailley M, et al. Mechanical tension and integrin alpha 2 beta 1 regulate fibroblast functions. J Investig Dermatol Symp Proc 2006;11:66–72.
33. Park CC, Zhang H, Pallavicini M, Gray JW, Baehner F, Park CJ, et al. Beta1 integrin inhibitory antibody induces apoptosis of breast cancer cells, inhibits growth, and distinguishes malignant from normal phenotype in three dimensional cultures and *in vivo*. Cancer Res 2006;66:1526–35.
34. Takada Y, Puzon W. Identification of a regulatory region of integrin-beta-1 subunit using activating and inhibiting antibodies. J Biol Chem 1993;268:17597–601.
35. Tokunou M, Niki T, Eguchi K, Iba S, Tsuda H, Yamada T, et al. c-MET expression in myofibroblasts - Role in autocrine activation and prognostic significance in lung adenocarcinoma. Am J Pathol 2001;158:1451–63.
36. Provenzano PP, Eliceiri KW, Campbell JM, Inman DR, White JG, Keely PJ. Collagen reorganization at the tumor-stromal interface facilitates local invasion. BMC Med 2006;4:38.
37. Xia H, Nho RS, Kahm J, Kleidon J, Henke CA. Focal adhesion kinase is upstream of phosphatidylinositol 3-kinase/Akt in regulating fibroblast survival in response to contraction of type I collagen matrices via a beta(1) integrin viability signaling pathway. J Biol Chem 2004;279:33024–34.
38. Dalla Costa AP, Clemente CFMZ, Carvalho HF, Carvalheira JB, Nadruz W Jr, Franchini KG. FAK mediates the activation of cardiac fibroblasts induced by mechanical stress through regulation of the mTOR complex. Cardiovasc Res 2010;86:421–31.
39. Margadant C, Monsuur HN, Norman JC, Sonnenberg A. Mechanisms of integrin activation and trafficking. Curr Opin Cell Biol 2011;23:607–14.
40. Bellis SL. Variant glycosylation: an underappreciated regulatory mechanism for beta 1 integrins. Biochim Biophys Acta 2004;1663:52–60.
41. Dingemans A-MC, van den Boogaart V, Vosse BA, van Suylen R-J, Griffioen AW, Thijssen VL. Integrin expression profiling identifies integrin alpha5 and beta1 as prognostic factors in early stage non–small cell lung cancer. Mol Cancer 2010;9:152.
42. Zhan J, Zhu X, Guo Y, Wang Y, Wang Y, Qiang G, et al. Opposite role of kindlin-1 and kindlin-2 in lung cancers. PLoS ONE 2012;7:e50313.
43. Wang F, Weaver VM, Petersen OW, Larabell CA, Dedhar S, Briand P, et al. Reciprocal interactions between beta1-integrin and epidermal growth factor receptor in three-dimensional basement membrane breast cultures: a different perspective in epithelial biology. Proc Natl Acad Sci U S A 1998;95:14821–6.
44. Planque C, Kulasingam V, Smith CR, Reckamp K, Goodglick L, Diamandis EP. Identification of five candidate lung cancer biomarkers by proteomics analysis of conditioned media of four lung cancer cell lines. Mol Cell Proteomics 2009;8:2746–58.

Downloaded from mcr.aacrjournals.org on September 15, 2015. © 2015 American Association for Cancer Research.

Published OnlineFirst October 3, 2014; DOI: 10.1158/1541-7786.MCR-14-0155

45. Reck M, Kaiser R, Mellemgaard A, Douillard J-Y, Orlov S, Krzakowski M, et al. Docetaxel plus nintedanib versus docetaxel plus placebo in patients with previously treated non–small cell lung cancer (LUME-Lung 1): a phase 3, double-blind, randomised controlled trial. Lancet Oncol 2014;15:143–55.
46. Mori T, Matsubara E, Fujino K, Shibata H, Yoshimoto K, Ikeda K, et al. Intra-tumor pressure of lung cancer may correlate tumor aggressiveness. J Thorac Oncol 2013;8:S429.
47. Barry-Hamilton V, Spangler R, Marshall D, McCauley S, Rodriguez HM, Oyasu M, et al. Allosteric inhibition of lysyl oxidase-like-2 impedes the development of a pathologic microenvironment. Nat Med 2010;16:1009–17.
48. Samuel MS, Lopez JI, McGhee EJ, Croft DR, Strachan D, Timpson P, et al. Actomyosin-mediated cellular tension drives increased tissue stiffness and beta-catenin activation to induce epidermal hyperplasia and tumor growth. Cancer Cell 2011;19:776–91.

Downloaded from mcr.aacrjournals.org on September 15, 2015. © 2015 American Association for Cancer Research.

Published OnlineFirst October 3, 2014; DOI: 10.1158/1541-7786.MCR-14-0155

AACR American Association for Cancer Research

Molecular Cancer Research

Matrix Stiffening and β_1 Integrin Drive Subtype-Specific Fibroblast Accumulation in Lung Cancer

Marta Puig, Roberto Lugo, Marta Gabasa, et al.

Mol Cancer Res 2015;13:161-173. Published OnlineFirst October 3, 2014.

Updated version Access the most recent version of this article at: doi:10.1158/1541-7786.MCR-14-0155

Cited articles This article cites 48 articles, 11 of which you can access for free at: http://mcr.aacrjournals.org/content/13/1/161.full.html#ref-list-1

E-mail alerts Sign up to receive free email-alerts related to this article or journal.

Reprints and Subscriptions To order reprints of this article or to subscribe to the journal, contact the AACR Publications Department at pubs@aacr.org.

Permissions To request permission to re-use all or part of this article, contact the AACR Publications Department at permissions@aacr.org.

Downloaded from mcr.aacrjournals.org on September 15, 2015. © 2015 American Association for Cancer Research.